Tunnel-injection quantum dot deep-ultraviolet light-emitting diodes with polarization-induced doping in III-nitride heterostructures

Jai Verma,[a] S. M. Islam, Vladimir Protasenko, Prem Kumar Kandaswamy, Huili (Grace) Xing, and Debdeep Jena
Department of Electrical Engineering, University of Notre Dame, Notre Dame, Indiana 46556, USA

(Received 12 November 2013; accepted 31 December 2013; published online 13 January 2014)

Efficient semiconductor optical emitters in the deep-ultraviolet spectral window are encountering some of the most deep rooted problems of semiconductor physics. In III-Nitride heterostructures, obtaining short-wavelength photon emission requires the use of wide bandgap high Al composition AlGaN active regions. High conductivity electron (n-) and hole (p-) injection layers of even higher bandgaps are necessary for electrical carrier injection. This approach requires the activation of very deep dopants in very wide bandgap semiconductors, which is a difficult task. In this work, an approach is proposed and experimentally demonstrated to counter the challenges. The active region of the heterostructure light emitting diode uses ultrasmall epitaxially grown GaN quantum dots. Remarkably, the optical emission energy from GaN is pushed from 365 nm (3.4 eV, the bulk bandgap) to below 240 nm (>5.2 eV) because of extreme quantum confinement in the dots. This is possible because of the peculiar bandstructure and band alignments in the GaN/AlN system. This active region design crucially enables two further innovations for efficient carrier injection: Tunnel injection of carriers and polarization-induced p-type doping. The combination of these three advances results in major boosts in electroluminescence in deep-ultraviolet light emitting diodes and lays the groundwork for electrically pumped short-wavelength lasers. © *2014 AIP Publishing LLC*. [http://dx.doi.org/10.1063/1.4862064]

Efficient electrically pumped semiconductor based optical emitters below 250 nm wavelength remains an unconquered territory. Several applications ranging from water purification, sterilization, integrated biosensors, solid state lighting, and lithography wait for such devices. The availability of low-power, lightweight, and robust deep-UV light sources are expected to seed several unforeseeable applications. Currently, III-nitride semiconductor materials are the prime contenders for this application. The optically active regions of such light emitters are composed of direct bandgap AlN ($E_g = 6.2$ eV, $\lambda = 200$ nm) and its alloy AlGaN with dilute concentrations of GaN ($E_g = 3.4$ eV, $\lambda =$ 365 nm). While the optically active regions are achievable with high internal quantum efficiencies,[1] injection of electrons and holes is a severe problem.

Light-emitting diodes (LEDs) and lasers in the visible regime of the spectrum with III-nitride semiconductors use GaN as the underlying substrate material, which is deposited on sapphire, Si, SiC, or used directly in the bulk crystal form. Deep-UV LEDs, on the other hand, require either sapphire or bulk AlN substrates to prevent reabsorption of the emitted photons.[2,3] Most of the device structure is Al(Ga)N, with high Al compositions to maintain optical transparency using a very large bandgap. Growth on sapphire results in high densities of dislocations that act as non-radiative recombination sites in the active region. Growth on bulk AlN crystals reduce this problem. But currently, bulk AlN crystals are either not easily available or have unintentional carrier doping. The free carrier absorption loss is severe through very thick bulk AlN layers. Methods to keep carriers from diffusing to defects can help make deep-UV LEDs more robust to substrates, like their visible counterparts. For electrical pumping, high densities of mobile electrons and holes are necessary. But due to large activation energies, donor (Si:AlN has $E_D \sim 280$ meV) and acceptor dopants (Mg:AlN has $E_A \sim 630$ meV) resist thermal ionization at room temperature.[4,5] Thus, the carrier injection layers are highly resistive. For this reason, Mg:GaN is used instead of Mg:AlN for hole injection—in spite of the large valence band offset with the active region and photon reabsorption in the p-contact layer. The p-type conductivity problem is so severe that just active regions pumped by an *external* electron beam shows a much higher net efficiency.[6]

In this work, we demonstrate a different approach for deep-UV LEDs. Instead of AlGaN active regions, the heterostructure uses GaN quantum dots under extreme quantum confinement embedded in an AlN matrix. The quantum confinement is so strong that photon emission occurs at ~5.3 eV from GaN, *remarkably blue shifted* from its bulk band-edge emission energy of 3.4 eV. Using high quantum confinement prevents carriers from diffusing to dislocations and makes the emission process robust to defects. Furthermore, the small thickness causes minimal quantum-confined Stark effect.[7–9] Using this layer, as the active region of the UV LED, opens the gates to simultaneously use two methods to solve the conductivity problem. Instead of conventional hot-carrier injection into quantum-well active regions, the injectors band edge states are aligned with the ground states of the quantum dots, and carriers are injected by tunneling. This allows us to shrink the bandgaps of the n- and p-regions, enhancing the electron and hole densities. Further, the p-injection region is compositionally graded to enhance

[a]Electronic mail: jverma@nd.edu

the conductivity by polarization-induced doping. This simultaneously solves two problems: It makes the p-layer conductive and allows for it to have a bandgap larger than the energy of the photons emitted from the active regions to avoid reabsorption. By combining these three designs in a single heterostructure, deep-UV LEDs are demonstrated with room-temperature electroluminescence (EL) at 243 nm.

The heterostructures discussed in this work are grown by plasma-assisted Molecular Beam Epitaxy (MBE). Epitaxial growth is performed on thick AlN-on-sapphire templates and monitored *in-situ* by reflection high-energy electron diffraction (RHEED). The AlN nucleation and buffer layers are grown under near-stoichiometric conditions at a substrate temperature of $T_c \sim 730\,^{\circ}\mathrm{C}$, an Al flux of 6.7×10^{-8} Torr, and a RF plasma power of 220 W resulting in a growth rate of ~0.18 Monolayers/s. The samples grown in these conditions exhibit very smooth surface morphology and corresponding streaky RHEED patterns, as shown in the inset of Fig. 1(a). The inset of Fig. 1(b) shows the active region heterostructure. GaN quantum dots are formed in the Stranski-Krastanov (SK) regime,[10–13] evidenced by the sharp transition from streaky to spotty RHEED patterns shown in the inset of Fig. 1(a). The Ga flux used is 6.2×10^{-8} Torr, which results in a N-rich growth condition. The driving force for the formation of the dots is the compressive strain due to the 2.4% lattice mismatch between AlN and GaN. Note that this transition is controllable during epitaxial growth; smooth pseudomorphic compressively strained GaN quantum wells have been demonstrated earlier and used for high-electron mobility transistors.[14,15] Our earlier report had discussed the bimodal distribution driven double-peak emission from the dots.[16] Here, we find that by successively reducing the GaN dot growth time from 35 to 25 s, the RT optical emission blue shifts from 270 nm to 246 nm as seen in the photoluminescence spectra A → B → C in Fig. 1(a). At the same time, the emission becomes single-peaked, showing a reduction in the bimodal size distribution and, in particular, the ~340 nm peak. Further, for sample D, by reducing the Ga flux from 6.2×10^{-8} Torr to 5.6×10^{-8} Torr while keeping the dot growth time constant at 25 s, the emission peak can be further blue-shifted to 238 nm.

Fig. 1(b) shows the PL spectra from GaN quantum dots grown in a *modified* SK mode.[12,13,17] This is achieved by growing the GaN quantum dots in a metal-rich regime (Ga flux: 2.6×10^{-7} Torr), as opposed to the N-rich dots of Fig. 1(a). The dot size is controlled by first growing the dots for 12 s followed by varying growth interrupts from 0 → 5 → 30 → 45 s. The interrupts make the dots smaller as evidenced by the blue shift of the room-temperature PL peak emission from 274 nm to 234 nm, the shortest wavelength corresponding to a photon energy of $\hbar\omega = 5.3$ eV. The corresponding decrease in the emission intensity indicates that the dots become smaller due to desorption rather than an Ostwald ripening process, resulting in a slight reduction of the active volume.

Photon emission energies, as high as, $\hbar\omega = 5.3$ eV from GaN, which has a bulk bandgap of $E_G = 3.4$ eV, are rather remarkable and merit discussion. All the quantum dot active regions have multiple dot layers separated by AlN barriers as indicated in the inset of Fig. 1(b). This is because they will form the active region of UV LEDs to enable tunnel-injection. Corresponding structural characterization by TEM and X-Ray diffraction shows dots of height $L_{\triangle} \sim 0.58$ nm and AlN barrier thicknesses 2.7 nm as discussed later. A simple infinite particle-in-a-box estimation of the quantization energy $\Delta E = \pi^2\hbar^2/2m^{\star}L_{\triangle}^2$ predicts *far more blue shifted* eigenvalues than experimentally observed, highlighting the extreme quantum confinement. The conduction bandstructure of GaN goes through an inflection point around 1 eV above the Γ−point minimum,[18] above which the effective mass turns negative. The intervalley separation in the conduction band is ≥ 2 eV, which provides a wide energy window for carrier injection into a single Γ-valley. The band offsets between GaN and the AlN barriers that confine carriers are $\Delta E_c \sim 2.1$ eV and $\Delta E_v \sim 0.7$ eV. These large intervalley separation and band offsets are unique to GaN and are crucial enablers of extreme quantum confinement and tunnel injection. To quantitatively explain the emission energy, a more refined model is necessary that accounts for the compressive strain, the bandstructure details, and the confinement potentials.

There are several advantages of using GaN quantum dots with extreme quantum confinement for deep-UV emission compared to AlGaN quantum wells. The three-dimensional confinement prevents electrons and holes from thermally diffusing to dislocations and recombining non-radiatively. The monolayer thickness makes the emission process robust to quantum-confined Stark-effect (QCSE). For example, in visible LEDs and lasers using InGaN quantum wells, the effect is so severe that non-polar or semi-polar growth orientations have been used to enhance the electron-hole wavefunction overlap to boost the oscillator

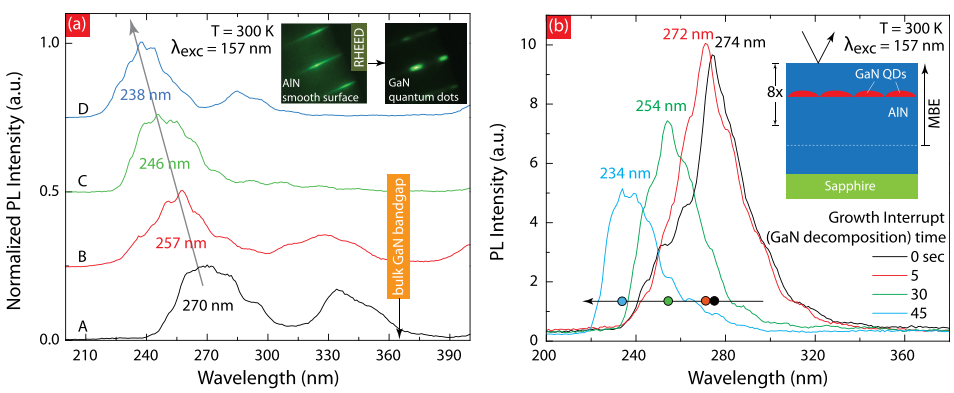

FIG. 1. (a) Photoluminescence spectra taken with an excimer laser ($\lambda_{exc} = 157$ nm) excitation show that the emission wavelength can be tuned by controlling the time and the Ga flux during the growth of the GaN quantum dots. (b) Room temperature photoluminescence spectra for quantum dots grown in a modified Stranski-Krastanov mode. The peak emission wavelength is blue-shifted as the growth interrupt (GaN decomposition) time is increased to make the GaN QDs smaller.

strength, by reducing the built-in electric field induced QCSE. An added advantage for LEDs is that the *direction* of the light emission is from the surface for GaN dots instead of the sides for AlGaN quantum wells. For AlGaN active regions with Al composition above 0.25,[19] the split-off valence band edge states become higher in energy than the light and heavy holes. Net angular momentum conservation in the optical transition process then forces the emitted light to be of a transverse magnetic (TM) polarization with $\mathbf{E}\|\langle 0001\rangle$, resulting in emission of light from the *edges* of the samples. For GaN active regions on the other hand, even under extreme quantum confinement, the emission is transverse electric (TE) with the electric field $\mathbf{E}\perp\langle 0001\rangle$,[20] which allows for easier light extraction from the surface. Next, we discuss the LED structures achieved by introducing electron and hole injection layers around the multilayer GaN quantum dot/AlN active regions.

Fig. 2 shows the fabricated LED device structure, a cross-section TEM image, and X-ray diffraction patterns of three devices used for demonstrating the innovative design. The active region of all three LEDs consists of 8-periods of the GaN quantum dot/AlN barrier heterostructure discussed earlier. For the LEDs I and II, the active region quantum dots were grown in the Stranski-Krastanov mode with 25 s growth time, whereas for LED III, the active region quantum dots were grown in the modified Stranski-Krastanov mode with 12 s growth time and 25 s ripening time. The n-injection layer for all three LEDs is a ~225 nm Si-doped high composition AlGaN with doping density $N_D \sim 5 \times 10^{19}/\text{cm}^3$. The p-injection region for the three LEDs is varied to demonstrate the effect of light reabsorption and polarization-induced doping. The layer composition details are highlighted in the measured X-ray diffraction patterns. Sample I has a uniform Mg-doped $Al_{0.5}Ga_{0.5}N$ as the p-contact layer and serves as the control sample. Samples II and III incorporate compositionally graded $Al_xGa_{1-x}N$ p-type layers. The linear grading is from $x = 0.5 \rightarrow 0.25$ for sample II and $x = 0.97 \rightarrow 0.77$ for sample III. These compositions are achieved by varying the Al metal flux during the MBE growth; because the flux depends exponentially on the effusion cell temperature $F_{Al} \propto \exp(-E_{Al}/k_B T_{Al})$ with an activation energy E_{Al}, the cell temperature T_{Al} is changed accordingly with time. The thickness of the p-layers was ~117 nm for all three samples, and the Mg doping was $N_A \sim 4 \times 10^{19}/\text{cm}^3$. The Z-contrast STEM cross-section image also shows the grading in the top p-layer and the n-AlGaN layer. The X-ray diffraction patterns show the realization of the LED heterostructures, along with the compositional grading.

After epitaxial growth, LEDs were fabricated by etching 200 nm deep mesas and depositing Ti/Al/Ni/Au metal stacks on the etched n-AlGaN surface for n-type contacts and thin Ni/Au thin transparent p-type current spreading layer on the mesa surface. Thicker Ti/Au probe pads were deposited on the p-contacts; a completed p-n junction LED structure with the quantum dot active region is shown in Fig. 2(a), with details of the metal stack thicknesses. The LEDs that were studied for electroluminescence were $300 \times 300\ \mu\text{m}^2$ in size.

Fig. 3 shows the cross-sections of the three LEDs in the first panel, the schematic energy band diagrams under forward bias in the second panel, and the corresponding room-temperature electroluminescence spectra from the three samples in the third. The energy-band diagram of sample I, the control sample, highlights the tunnel injection process, as well as the problem of reabsorption of emitted photons. The GaN quantum dot active region is separated from the electron and hole injection regions by AlN barriers. The conduction band edge of the n-AlGaN on the right is aligned with the ground state eigenvalue of the quantum dot under forward bias, and electrons are thus injected by tunneling through the AlN. A similar process occurs for holes in the valence band from the p-injection layer. Note that traditional UV LEDs inject carriers by drift/diffusion transport into quantum wells, and the excess energy $E_{exc} = (E_c^n - E_{c0}^{QW}) + (E_{v0}^{QW} - E_v^p)$ is irretrievably lost to heat by optical phonon emission as the carriers relax to the ground states of the active region. This also results in heating of the active region, which is responsible for lateral thermal diffusion of carriers to non-radiative sites in quantum wells. Heat is also responsible for the thermal degradation of LEDs. Tunnel injection into quantum dots avoids these issues. In addition, since the valence band offset ΔE_v is smaller than the conduction band offset ΔE_c, the tunnel-injection process affords a natural offset to the effective mass and mobility mismatch between electrons and holes by enabling a balanced carrier injection into the active region.

However, the control sample I also highlights the problem of the p-type injection layer. Electrons tunnel efficiently

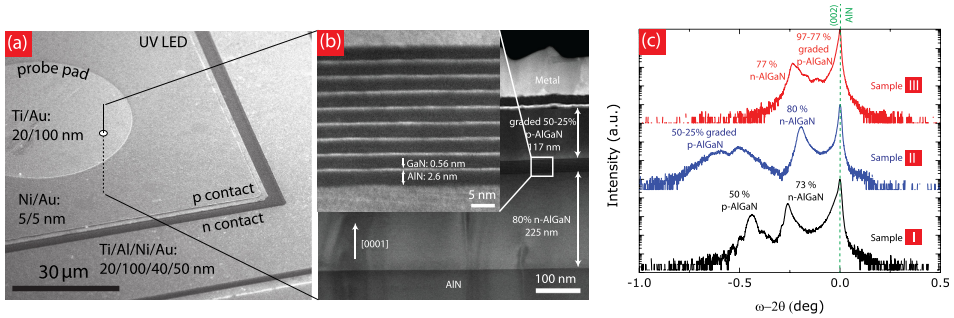

FIG. 2. (a) SEM micrograph of processed LED structure showing the metal contacts and the mesa. (b) STEM micrograph of the processed GaN QD LED structure. The GaN QDs are 0.56 nm in thickness while the AlN barrier is 2.6 nm. The GaN layers appear to be continuous due to superimposition of GaN QDs in the cross-section sample used for STEM imaging. (c) Triple axis ω-2θ scans showing the difference in graded AlGaN LED structure and non-graded AlGaN LED structure.

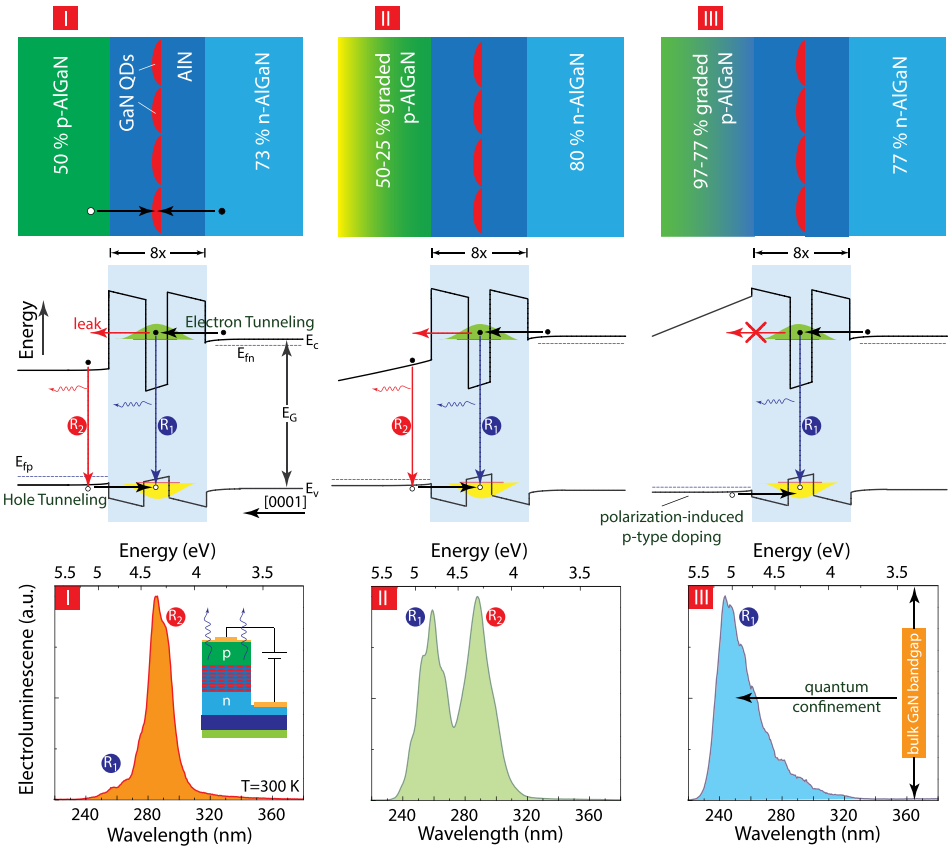

FIG. 3. Schematic cross-section of GaN/AlN QD UV LEDs. Sample I: 73% n-AlGaN, 50% p-AlGaN; sample II: 80% n-AlGaN, 50%–25% p-AlGaN; sample III: 77% n-AlGaN, 97%–77% p-AlGaN. Corresponding schematic band diagrams at forward bias showing the tunneling transport and recombination mechanisms in QDs (R_1) and the AlGaN cladding layer (R_2). Individual EL spectra for the 3 structures show short and long wavelength emissions.

across the active region and leak into the p-AlGaN region as indicated in Fig. 3. They then radiatively recombine there with holes leading to emission at the bandgap energy of that layer corresponding to the peak R_2 shown in the EL spectra in the third panel. The photons produced by recombination in the GaN quantum dots have a higher energy R_1; so they are re-absorbed in p-AlGaN layer and are further down-converted to R_2. Thus, control sample I exhibits a strong EL peak at $\lambda_2 = 290$ nm ($\hbar\omega_1 = 4.3$ eV) corresponding to process R_2. The feeble R_1 peak is masked by the two R_2 emission processes.

In sample II, the Al composition in the p-AlGaN layer is linearly graded down from 50% to 25% to take advantage of polarization-induced p-type doping. The expected polarization-induced doping is $\rho_\pi = -\nabla \cdot \mathbf{P} \sim 9.4 \times 10^{17}/\text{cm}^3$. The concept of polarization-induced doping has been demonstrated in several recent reports.[21–23] Here, this concept is demonstrated in a deep-UV LED. As a result of an enhanced hole density, the *net* EL emission intensity is significantly enhanced compared to the control sample, as will be discussed shortly. In Fig. 3, the EL spectra shows a strong R_1 peak at $\lambda_1 = 259$ nm ($\hbar\omega_1 = 4.8$ eV) in addition to the same R_2 peak as sample I. The reason for the two peaks is clear from the energy band diagram: Significant down-conversion occurs in sample II. In spite of the polarization-induced doping boost in hole concentration, significant electron leakage into this layer and reabsorption of

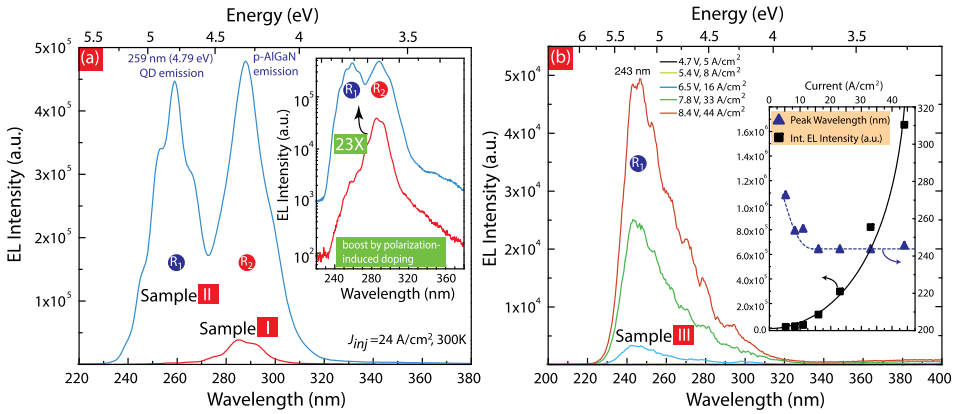

FIG. 4. (a) EL spectra for graded AlGaN layer LED (sample II) showing emission from QDs (259 nm) and p-AlGaN layer (290 nm). The non-graded AlGaN layer LED (sample I) shows weak QD emission. The EL intensity from sample II is 23 times larger than that from sample I, implying better hole concentration due to polarization induced doping. Inset: EL spectra in log scale. (b) EL spectra for 97%–77% graded AlGaN layer LED (sample III) showing 243 nm emission from GaN QDs grown in modified SK mode. Inset: EL peak wavelength and intensity variation with injection current density. The peak wavelength becomes constant on increasing the current density. The long wavelength peaks at low injection current density can be attributed to emission from large size GaN QDs present in the active region due to size inhomogeneity.

R_1 photons, both, result in a strong R_2 peak. If the electron leakage could be reduced and light reabsorption be avoided, a single deep-UV peak will result.

These two problems are solved in sample III. The p-AlGaN layer in sample III is compositionally graded from 97% to 77%, which leads to a polarization-induced doping $\rho_\pi = -\nabla \cdot \mathbf{P} \sim 1.2 \times 10^{18}/\text{cm}^3$. More crucially, it (a) introduces an energy gap in the path of electrons that could have leaked into the p-AlGaN cap layer and (b) simultaneously makes the bandgap of the p-AlGaN cap layer larger than the optical transition energy of the quantum-dot active region R_1, preventing reabsorption. This results in a single peak emission at $\lambda_1 = 243$ nm, ($\hbar\omega_1 = 5.1$ eV), as shown in the room-temperature EL spectra in the third panel in Fig. 3. Evidently, this results from process R_1 in the quantum dot active regions, and there is no prominent longer-wavelength peak. In the figure showing the EL spectra from sample III, the bulk bandgap of GaN is also indicated. The remarkably large blue-shifted single peak quantum-dot emission that is observed in the PL spectra carries over to the EL spectra at room temperature; it is unmasked by polarization-induced doping of the p-type layer.

In Fig. 4(a), the electroluminescence spectra of samples I and II are compared. Polarization-induced p-type doping boosts the integrated EL emission intensity from sample II by 23 times compared to sample I at an injection current level of $J_{inj} \sim 24$ A/cm^2. Fig. 4(b) shows the single-peak EL spectra from sample III at various current injection levels. The emission remains single peaked, and the integrated EL intensity increases sharply with injection current. At the lowest injection currents, the emission peak is red-shifted. This could be attributed to size inhomogeneity of the quantum dots: The largest dots will fill first by tunneling, because they have the lowest ground state energies. However, above a current injection density of $J_{inj} \sim 15$ A/cm^2, the peak emission stabilizes to $\lambda = 243$ nm, accompanied by a corresponding increase in the integrated EL intensity.

In summary, we demonstrate that sub 250 nm deep-UV emission can be obtained from GaN quantum dots in the extreme quantum-confinement limit at room temperature by electrical injection. The GaN active region comprising of ultrasmall GaN dots embedded in an AlN matrix enables tunnel-injection of carriers from the n- and p-injection regions. Quantum confinement prevents lateral diffusion of carriers to non-radiative recombination sites, and tunnel-injection enables a balanced injection of electrons and holes. The design also incorporates polarization-induced doping for simultaneously improving p-type doping, and preventing reabsorption of the deep-UV photons emitted from the quantum dots. The demonstration thus paves the way to improve radiative recombination, lower heat generation, improved light extraction, and more efficient doping, all of which remain major roadblocks to improve the efficiency of deep-UV LEDs. The tunnel-injection quantum dot UV LEDs with polarization-induced doping presented are, by no means, the best heterostructure design; it can be vastly improved upon by carefully examining the effect of the number of periods in the active region and improving the ohmic contacts to the p-type layer. Truly, temperature-independent operation of deep-UV LEDs can also be obtained by incorporating polarization-induced doping in the n-type AlGaN layer as well. All the heterostructures discussed in this work were of a metal-polar orientation. Graded AlGaN regions also result in graded refractive indices, which enable confinement of optical modes. Combining the active region design developed in this work with growth along the N-polar orientation is a feasible approach towards graded-index separate confinement heterostructure (GRINSCH) lasers operating in the deep-UV regime in the future. The techniques demonstrated in this work lay the path towards that goal.

[1]A. Bhattacharyya, T. D. Moustakas, L. Zhou, D. J. Smith, and W. Hug, Appl. Phys. Lett. **94**, 181907 (2009).
[2]A. Khan, K. Balakrishnan, and T. Katona, Nat. Photonics **2**, 77 (2008).
[3]M. Kneissl, T. Kolbe, C. Chua, V. Kueller, N. Lobo, J. Stellmach, A. Knauer, H. Rodriguez, S. Einfeldt, Z. Yang, N. M. Johnson, and M. Weyers, Semicond. Sci. Technol. **26**, 014036 (2011).
[4]P. Kozodoy, H. Xing, S. P. DenBaars, U. K. Mishra, A. Saxler, R. Perrin, S. Elhamri, and W. C. Mitchel, J. Appl. Phys. **87**, 1832 (2000).
[5]Y. Taniyasu, M. Kasu, and T. Makimoto, Nature **441**, 325 (2006).
[6]T. Oto, R. G. Banal, K. Kataoka, M. Funato, and Y. Kawakami, Nat. Photonics **4**, 767 (2010).
[7]D. A. B. Miller, D. S. Chemla, T. C. Damen, A. C. Gossard, W. Wiegmann, T. H. Wood, and C. A. Burrus, Phys. Rev. Lett. **53**, 2173 (1984).
[8]T. Takeuchi, S. Sota, M. Katsuragawa, M. Komori, H. Takeuchi, H. Amano, and I. Akasaki, Jpn. J. Appl. Phys., Part 2 **36**, L382 (1997).
[9]F. Bernardini and V. Fiorentini, Phys. Status Solidi A **190**, 65 (2002).
[10]B. Daudin, F. Widmann, G. Feuillet, Y. Samson, M. Arlery, and J. L. Rouvière, Phys. Rev. B **56**, R7069 (1997).
[11]C. Adelmann, J. Simon, G. Feuillet, N. T. Pelekanos, B. Daudin, and G. Fishman, Appl. Phys. Lett. **76**, 1570 (2000).
[12]J. S. Brown, P. M. Petroff, F. Wu, and J. S. Speck, Jpn. J. Appl. Phys., Part 2 **45**, L669 (2006).
[13]J. Renard, P. K. Kandaswamy, E. Monroy, and B. Gayral, Appl. Phys. Lett. **95**, 131903 (2009).
[14]Y. Taniyasu and M. Kasu, Appl. Phys. Lett. **99**, 251112 (2011).
[15]G. Li, R. Wang, J. Guo, J. Verma, Z. Hu, Y. Yue, F. Faria, Y. Cao, M. Kelly, T. Kosel, H. Xing, and D. Jena, IEEE Electron Device Lett. **33**, 661 (2012).
[16]J. Verma, P. Kandaswamy, V. Protasenko, A. Verma, H. Xing, and D. Jena, Appl. Phys. Lett. **102**, 041103 (2013).
[17]F. Widmann, J. Simon, B. Daudin, G. Feuillet, J. L. Rouvière, N. T. Pelekanos, and G. Fishman, Phys. Rev. B **58**, R15989 (1998).
[18]A. Konar, A. Verma, T. Fang, P. Zhao, R. Jana, and D. Jena, Semicond. Sci. Technol. **27**, 024018 (2012).
[19]K. B. Nam, J. Li, M. L. Nakarmi, J. Y. Lin, and H. X. Jiang, Appl. Phys. Lett. **84**, 5264 (2004).
[20]P. Strak, P. Kempisty, M. Ptasinska, and S. Krukowski, J. Appl. Phys. **113**, 193706 (2013).
[21]D. Jena, S. Heikman, D. Green, D. Buttari, R. Coffie, H. Xing, S. Keller, S. DenBaars, J. S. Speck, U. K. Mishra, and I. Smorchkova, Appl. Phys. Lett. **81**, 4395 (2002).
[22]S. Li, T. Zhang, J. Wu, Y. Yang, Z. Wang, Z. Wu, Z. Chen, and Y. Jiang, Appl. Phys. Lett. **102**, 062108 (2013).
[23]J. Simon, V. Protasenko, C. Lian, H. Xing, and D. Jena, Science **327**, 60 (2010).